Materials Today Bio 26 (2024) 101092

Contents lists available at ScienceDirect

Materials Today Bio

journal homepage: www.journals.elsevier.com/materials-today-bio

Injectable and high-strength PLGA/CPC loaded ALN/MgO bone cement for bone regeneration by facilitating osteogenesis and inhibiting osteoclastogenesis in osteoporotic bone defects

Lei Huang [a], Peihao Cai [b], Mengxuan Bian [a], Jieqin Yu [c], Lan Xiao [d], Shunyi Lu [a], Jiayi Wang [a], Weisin Chen [a], Guanjie Han [a], Xingdong Xiang [a], Xin Liu [b], Libo Jiang [a,***], Yulin Li [b,**], Jian Zhang [a,*]

[a] *Department of Orthopedic Surgery, Zhongshan Hospital, Fudan University, Shanghai, 200032, China*
[b] *The Key Laboratory for Ultrafine Materials of Ministry of Education, Frontiers Science Center for Materiobiology and Dynamic Chemistry, Engineering Research Center for Biomedical Materials of Ministry of Education, School of Materials Science and Engineering, East China University of Science and Technology, Shanghai, 200237, China*
[c] *Department of Orthopedic Surgery, Zhejiang Provincial Hospital of Chinese Medicine, Hangzhou, Zhejiang Province, 310003, China*
[d] *School of Medicine and Dentistry, Griffith University, Gold COast, QLD, 4222, Australia*

A R T I C L E I N F O

Keywords:
Osteoporosis
Bone regeneration
Injectable calcium phosphate cement
PLGA nanofiber

A B S T R A C T

Osteoporosis (OP) can result in slower bone regeneration than the normal condition due to the imbalance between osteogenesis and osteoclastogenesis, making osteoporotic bone defects healing a significant clinical challenge. Calcium phosphate cement (CPC) is a promising bone substitute material due to its good osteoinductive activity, however, the drawbacks such as fragility, slow degradation rate and incapability to control bone loss restrict its application in osteoporotic bone defects treatment. Currently, we developed the PLGA electrospun nanofiber sheets to carry alendronate (ALN) and magnesium oxide nanoparticle (nMgO) into CPC, therefore, to obtain a high-strength bone cement (C/AM-PL/C). The C/AM-PL/C bone cement had high mechanical strength, anti-washout ability, good injection performance and drug sustained release capacity. More importantly, the C/AM-PL/C cement promoted the osteogenic differentiation of bone marrow mesenchymal stem cells and neovascularization via the release of Mg^{2+} (from nMgO) and Ca^{2+} (during the degradation of CPC), and inhibited osteoclastogenesis via the release of ALN *in vitro*. Moreover, the injection of C/AM-PL/C cement significantly improved bone healing in an OP model with femur condyle defects *in vivo*. Altogether, the injectable C/AM-PL/C cement could facilitate osteoporotic bone regeneration, demonstrating its capacity as a promising candidate for treatment of osteoporotic bone defects.

1. Introduction

Osteoporosis (OP) is one of the most common bone diseases characterized by bone loss and destruction of bone microstructure, leading to elevated bone fragility and an increased risk of fracture [1]. In recent years, bone loss-associated fractures, due to the rapid growth of the elderly population, has become a global health issue, causing a significant impact on patients' life quality and huge socio-economic burden [2–4]. In the case of OP, due to the disorder between bone formation/osteogenesis and bone resorption/osteoclastogenesis balance, it is more difficult to induce bone regeneration which has become one of the major challenges in clinical treatment [5,6]. Currently, poly (methyl methacrylate) (PMMA) bone cement is used as the main approach for treating osteoporotic fractures due to its good injectability and mechanical properties after curing, however, it has significant disadvantages such as unnecessary thermal damage, leakage of bone cement and cytotoxic monomers, causing secondary damage to the patient [7,8]. Moreover, PMMA is unable to regulate the

* Corresponding author. Department of Orthopedic, Zhongshan Hospital, Fudan University, Shanghai, 200032, China.
** Corresponding author.
*** Corresponding author. Department of Orthopedic, Zhongshan Hospital, Fudan University, Shanghai, 200032, China.
E-mail addresses: jiang.libo@zs-hospital.sh.cn (L. Jiang), yulinli@ecust.edu.cn (Y. Li), zhang.jian@zs-hospital.sh.cn (J. Zhang).

https://doi.org/10.1016/j.mtbio.2024.101092
Received 9 January 2024; Received in revised form 18 April 2024; Accepted 14 May 2024
Available online 25 May 2024

osteogenesis-osteoclastogenesis balance, which is one of the major limitations of PMMA in the treatment of osteoporotic fracture.

Calcium phosphate cement (CPC) is considered as one of the bone substitute materials with promising translational potential, due to its similar composition to the bone tissue, good osteo-inductive capacity, plasticity, and biocompatibility [9,10]. However, the application of traditional CPC is limited by its fragility, slow degradation rate and lack of the capacity to inhibit osteoclastogenesis in OP-related fracture [11,12]. In our previous study, we fabricated an injectable nanofiber-reinforced CPC, by introducing Poly (lactide-co-glycolic acid) (PLGA) and carboxymethyl cellulose (CMC) into CPC (to generate C/PL/C) to facilitate the osteogenic capacity of the bone cement [13]. Nevertheless, this strategy should be improved for osteoporotic bone regeneration, since its design did not take into account the imbalance between osteogenesis and osteoclastogenesis. Therefore, it is of great significance to develop novel bone materials that can effectively treat fractures in osteoporotic conditions.

Alendronate (ALN), a commonly used anti-OP drug, is a nitrogen-containing bisphosphonate that binds to the bone surface and inhibits bone resorption by osteoclasts [14]. However, the oral administration of ALN may lead to a series of gastrointestinal reactions and low bioavailability (only 0.6 %), suggesting the necessity to apply ALN without oral administration [15,16]. Previous studies have reported that adding ALN to CPC will seriously impair the curing process of CPC, which significantly limits the loading of ALN in CPC and cannot effectively promote OP-related bone formation [17]. Studies also showed that the setting time of CPC remained within the acceptable range for clinical use when the concentration of ALN was below 0.1 wt% [18]. Meanwhile, PLGA can prevent high concentrations of ALN from direct contact with the uncured CPC [19]. Herein, a new design strategy was proposed to develop a ALN-loaded PLGA nanofiber sheets with injectable bone cement which can regulate osteogenic-osteoclast balance. In addition, magnesium oxide nanoparticle (nMgO) was loaded with ALN into the injectable bone cement to further facilitate bone regeneration in OP, owing to the good osteo-inductivity and angiogenic capacity of Mg^{2+} [20,21].

To avoid the effects of direct addition of ALN and nMgO to CPC on curing, in this study, PLGA fibers were used as the carrier of ALN and nMgO to eliminate the effects of direct contact of ALN and nMgO with CPC. The drug-loaded nanofiber sheets with two-dimensional structure were prepared by electrospinning and mechanical milling. The two-dimensional network not only improved the material mechanical strength and CPC degradation but also had the potential to promote bone and vascular regeneration by sustained-releasing Mg^{2+}, meanwhile, it inhibited osteoclastogenesis by releasing ALN, thereby synergistically facilitating bone regeneration in OP-related bone defects. Moreover, PLGA nanofiber sheets could reduce the negative impact of ALN on CPC by controlled releasing ALN. The physicochemical properties of the composite bone cement, including drug release, degradability, and ion release, were characterized. Further, the effects of material on osteogenic differentiation of bone marrow mesenchymal stem cells (BMSCs) and its inhibitory effects on osteoclast formation were explored, followed with the effects on osseointegration and bone regeneration in OP rat models *in vivo*. Our results suggest that the developed bone cement can be considered as the next generation of injectable bone regeneration materials for the treatment of osteoporosis-associated bone defects (Scheme 1).

2. Materials and methods

2.1. Fabrication of injectable drug-loaded nanofibers sheet composite bone cement

Nanofiber sheets containing magnesium oxide nanoparticle (nMgO, Aladdin, China, 30 nm) and alendronate (ALN, Yuanye, China) are prepared by crushing nanofibrous membranes prepared by electrospinning. PLGA (70: 30 lactide: glycolide, $M_w = 10$ kDa) was dissolved in the mixed solvent of tetra-hydrofuran (THF)/N, N-dimethylformamide (DMF) (v/v = 3:1) with a concentration of 25 % (w/v) [22]. Subsequently, the ALN (5 wt % relative to PLGA) and nMgO (1 wt % relative to PLGA) were added to PLGA solution and stirred for 2 h to get homogeneous solutions. The membranes were prepared with a commercial electrospinning equipment (Foshan Light Son, E02-001, China) using a 20 G blunt needle. The electrospinning parameters were set at a collection distance of 10 cm, flow rate of 1.0 mL/h and applied voltage of 22 kV. The membranes containing ALN and both ALN and nMgO were termed as ALN/PLGA (A-PLGA) and ALN/nMgO/PLGA (AM-PLGA), respectively. The formed fibrous mats were cut into 2 × 2 cm^2 pieces

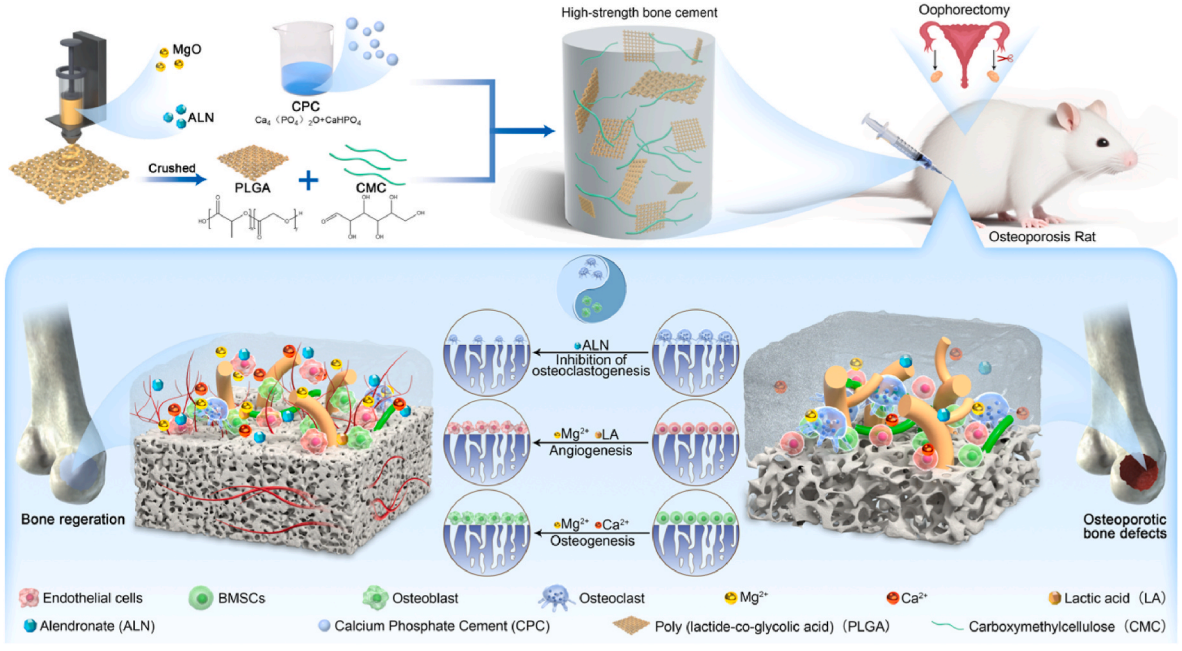

Scheme 1. Schematic representation of fabricating C/AM-PL/C injectable high-strength bone cement for bone regeneration in the osteoporosis. The detailed method and process of fabricating C/AM-PL/C bone cement and the mechanism of bone regeneration at bone defects by the injectable high-strength bone cement.

with scissors. These pieces and 1 L ethanol are added to a cutter, cut and sieved to the right size (< 1 mm) for gaining nanofiber sheets. Finally, the sheets were dried in a vacuum oven at 40 °C for 3 h. Calcium phosphate cement (CPC, Rebone Company, China) powder was composed of dicalcium phosphate anhydrous (DCPA, $CaHPO_4$) and tetracalcium phosphate (TTCP, $Ca_4(PO_4)_2O$). The solid phase of the bone cement was prepared by mixing CPC, PLGA nanofiber sheets and carboxymethyl cellulose (CMC) in a certain mass ratio (Table S1). Then pastes were fabricated by mixing the solid-phase composite solutions of citric acid, sodium citrate and sodium hydrogen phosphate, etc. (supplied by the Rebone company), at a liquid/powder ratio of 0.45.

2.2. Setting time, injectability and mechanical properties

The paste was made by mixing 1.5 g of various cement powders with 0.675 mL of curing fluid, which was then filled into Teflon moulds (Ø 6 × 12 mm). The cements were placed in a chamber (100 % humidity and 37 °C) to cure. The curing time was measured by a Vicat apparatus, according to the ASTM Test Method C 187-98. The sample was measured every 0.5 min to indicate whether setting or not [23,24]. After hardening for 72 h, all samples (n = 5) were polished on both sides. Cylindrical samples were measured at a loading rate of 1 mm/min using a universal testing machine (SANS CMT 2503, MTS Industrial Systems, USA).

The injectability of CPC was analyzed according to the previous protocol [25]. Each cement (n = 5) was prepared by manually mixing the solid phase and liquid for 1 min with the aid of a plastic knife and then filled in the 1 mL syringe (Yuekang, China) for injectability evaluation. Injectability was calculated based on the mass percentage of paste remaining in the syringe after injection. Three replicates were carried out for each group according to equation [1].

$$I = \frac{M_1 - M_2}{M_1}\% \quad (1)$$

where I indicated injectability. M_2 corresponds to the mass of paste which remains in the syringe and cannula after extrusion and M_1 corresponds to the mass of paste before extrusion.

2.3. Chemical phase structure and surface morphology

The membrane and cement samples were characterized by X-ray diffraction (XRD, 18KW/D/max2550VB/PC, Japan) with Cu K_α radiation and Ni filter (λ = 1.5406 A, 100 mA, 40 kV) in a continuous scan mode. The diffraction data were collected from 10 to 80°, with a step size of 0.02° per step at a scan speed of 10 min^{-1} and Fourier Infrared Spectrometer (FTIR, Nicolet is50, Japan) with a resolution of 4 cm^{-1} and 32 scans. Surface morphology of membrane and cement samples, the energy dispersive spectrometer (EDS) elements analysis and mapping of carbon, nitrogen and magnesium were examined with field emission scanning electron microcopy at 15 kV (SEM, S-4800, Japan).

The incorporation of nMgO and ALN within PLGA nanofiber was also observed by transmission electron microscopy (TEM, Hitachi, H-800, Japan) at 200 kV, and the EDS elements analysis and mapping of magnesium and nitrogen (Fig. S1). Water contact angles were measured on the surface of membranes using contact angle equipment (Changchun No.5 Optical Instrument Co., Ltd., China).

2.4. Characterization of material porosity change and ionic release

The effect of each component on the porosity of the cement was tested by mercury intrusion porosimetry [26]. Porosity of the specimens (Ø 6 × 12 mm, n = 3) were assessed by mercury intrusion porosimetry using Auto Pore 9510 porosimeter (Micrometrics, USA).

The release of Ca^{2+}/Mg^{2+} from the composite cement was examined. In brief, the samples of all groups (n = 3) were soaking in 5 mL PBS solution (pH = 7.4). After 1, 3, 5, 7, 14 days, the soaking solution was collected. The concentrations of Ca^{2+} and Mg^{2+} of the solution were measured with inductively coupled plasma atomic emission spectrometer (ICP-AES, Perkin-Elmer Optima 2000, USA) with wavelength range 175–900 nm.

2.5. pH values of cement-soaking solution

The pH of the soaking solution had been monitored until the sample was degraded. In brief, the samples of all groups (n = 3) were immersed in 5 mL PBS solution. After 1, 3, 5, 7, 14 days, the pH of the immersion solution was measured using a pH meter (Mettler Toledo, China).

2.6. Characterization of ALN release

The release of ALN was determined by immersing the samples in 5 mL of PBS solution and incubating at 37 °C and 80 rpm according to a previous protocol, and the concentration of ALN in the soaking solution was determined using the ninhydrin assay for 1, 3, 5, 7, 14, 21, 28, 35, 42, 49, and 56 days after the cement had been immersed [27]. Five sets of 10 mL ALN solutions of different concentrations were configured to develop color using ninhydrin, and then a standard curve was obtained using a spectrophotometer [28].

2.7. Evaluation of in vitro sample degradation

The specimens from all groups (n = 3) were drained in a solution of Tris(hydroxymethyl) aminomethane-HCl (Tris-HCl) (pH = 7.4) at 37 °C. Samples were taken out of solution after being immersed for 1 days, 3 days, 5 days, 7 days, 14 days, 30 days, 60 days, 90 days, washed with deionized water and dried in a blast dryer at 60 °C for 2 h. The percentage of weight loss was calculated as equation [2].

$$\text{Weight loss}(\%) = \frac{W_0 - W_t}{W_0} \times 100\ \% \quad (3)$$

where W_0 is the start mass and W_t indicates mass at time t.

2.8. In vitro osteogenesis assay

2.8.1. Cell culture

The Fudan University Animal Care and Use Committee (Shanghai, China) approved the protocol for the animal experiments. Bone marrow mesenchymal stem cells (BMSCs) from four to eight-week-old Sprague-Dawley rats (SD rats) were obtained from Shanghai JieSiJie Laboratory Animals Co., LTD. BMSCs were harvested from the femur and tibia of rats according to the published protocol [29]. BMSCs were cultured in MEM Alpha Medium (α-MEM, Gibco, USA) with 10 % fetal bovine serum (FBS, BI, USA) and 1 % penicillin and streptomycin (Sigma, USA). The media was changed every two days. When cells reached 80–90 % confluence, BMSCs were passaged and cells within 2–4 passages were used in the subsequent experiments. To test the BMSC responses to materials, all cement samples were sterilized by soaking in 75 % alcohol for 24 h. Then, all samples were washed with PBS for three times and immersed in α-MEM with 10 % FBS at 37 °C for 24 h to obtain the cement extracts.

2.8.2. Cell proliferation and adhesion

According to ISO 10993, CPC, C/PL/C, C/A-PL/C, C/AM-PL/C sample (10 mm × 3 mm) extracts were used to test the cytotoxicity [13]. For cell counting kit-8 (CCK-8) assay, BMSCs with the density of 5×10^4 cells/well were seeded on tablet samples (3 mm in height × 10 mm in diameter) of each group immersed in α-MEM medium in a 24-well culture plate. After culturing for 1, 4, 7 days, the medium were replaced with α-MEM medium containing 10 % CCK-8 solution (Beyotime Biotechnology, China). The plate then subsequently incubated at 37 °C

in 5 % CO^2 and read the plate at the absorbance at 450 nm using a microplate reader (Epoch, BioTek Instruments, Inc.)

For Live/Dead staining assay, BMSCs were treated with the cement extracts for 1/4/7 days and then stained with the Calcein-AM/PI double stain-kit according to the manual (Beyotime Biotechnology, China). The samples were observed and imaged by using an inverted fluorescence microscope (Olympus, IX71, Japan).

For SEM observation, BMSCs were seeded on the tablet samples in a 24-well culture plate at 5×10^4 cells/well as mentioned above. After culturing for 3 days, the cells were fixed with 2.5 % glutaraldehyde, dehydrated, and allowed to air-dry overnight and then analyzed with SEM (S-4800, Hitachi, Japan).

2.8.3. Osteogenic differentiation

For osteogenic differentiation experiments, osteogenesis inducing medium (OIM) were made by supplementing the normal culture medium with 0.05 mM vitamin C (Sigma, USA), 10 mM β-glycerophosphate (Sigma, USA) and 10 nM dexamethasone (Sigma, USA). In detail, BMSCs were cultured in a 12-well plate with normal cement extracts at 1×10^5 cells/well in the incubator. When cell density reached 70–80 % approximately, the medium was replaced with OIM. OIM were exchanged every 3 days and the osteogenic differentiation of BMSCs was assessed with alkaline phosphatase (ALP) staining and ALP activity after 7/14 days, as well as alizarin red S (ARS) staining after 21 days.

For ALP staining, a BCIP/NBT solution (Beyotime Biotechnology, China) was used. After 7/14 days of culture, cell monolayers were washed twice with PBS and were processed with 10 % neutrophilic formalin for 15 min. After washing twice with PBS, the samples were stained according to the manufacturer's protocol and observed with a light microscope (Olympus, IX71, Japan). ALP activity was quantified using an ALP assay kit (Beyotime Biotechnology, China) after 7/14 days of culture. Briefly, BMSCs were lysed using RIPA lysis buffer (Beyotime Biotechnology, China) and centrifuged at 3000 rpm for 20 min and the ALP activity assay was performed referred to the kit protocol. The total cellular protein was quantified simultaneously using a BCA protein assay kit according to the protocol (Beyotime Biotechnology, China). ALP activity was determined after measuring the absorbance at 405 nm on a microplate reader (Epoch, BioTek Instruments, Inc.)

For Alizarin red S (ARS) staining assay to assess mineralization (Beyotime Biotechnology, China), after 21 days of OIM treatment, 0.5 % alizarin red working solution was performed to evaluate the calcium deposition referred to the manufacturer's instructions and visualized with optical microscope (Olympus, IX71, Japan).

2.8.4. Osteogenic-related gene levels

After being treated with OIM for 7 days, all samples were harvested by using 1 mL Trizol RNA extract kit (Invitrogen, Carlsbad, CA) to extract the total RNA. A Revert Aid First Strand cDNA Synthesis Kit (Thermo Fisher Scientific) was used to reverse-transcribe the RNA into cDNA. RT-PCR was performed to evaluate the osteogenesis-related genes expression (ALP, BMP-4, COL-1, OCN, Osterix, and Runx-2; β-actin as reference). Primer sequences information is listed in Table S2.

2.8.5. Osteogenesis-related protein levels

After culturing with extracts in OIM for 7 days, BMSCs were lysed on ice in RIPA buffer mixed with phenylmethylsulfonyl fluoride (PMSF, 100 mM). The lysates were centrifuged at 10,000 rpm for 10 min and the total protein concentration was detected according to the bicinchoninic acid (BCA) protocol (Beyotime Biotechnology, China). Western blotting was performed as follows: Equivalent amounts of proteins were separated through SDS-polyacrylamide gel electrophoresis (12.5 % or 15.0 %) and transferred onto a polyvinylidene fluoride membrane (PVDF, Millipore, Darmstadt, German). After that, membranes were blocked with 5.0 % skimmed milk for 1 h and then incubated with the following primary antibodies: anti-GAPDH (1:1000), anti-osteopontin (OPN, 1:1000), anti-runt-related transcription factor 2 (Runx-2, 1:1000), anti-osteocalcin (OCN, 1:1000) at 4 °C overnight. After being washed with Tris-HCl Buffer Saline and Tween (TBST) for three times, the membrane was incubated with secondary antibodies (HRP-labeled, 1:2000) for 1 h. After being washed with TBST, the protein signals were visualized using the enhanced chemiluminescence system reagent (Beyotime Biotechnology, China) and protein quantification was performed using Image J software.

2.9. Osteoclasts inhibition assay

2.9.1. Cell culture

In this study, RAW264.7 cell line obtained from the Cell Bank of Shanghai Institutes for Biological Sciences were used to induce osteoclasts. RAW264.7 cells were cultured in DMEM/High glucose (HG-DMEM, Gibco, USA) with 10 % fetal bovine serum (FBS, BI, USA) and 1 % penicillin and streptomycin (Sigma, USA). The media was changed every two days. When cells reached 80–90 % confluence, cells were passaged and cells within 2–4 passages were used in subsequent experiments.

2.9.2. Cell viability

For assessing the effect of ALN on osteoclasts viability, RAW 164.7 cells were cultured with extracts in 10 % RANKL (100 ng/mL) solution for 7 days. The CCK-8 assay was performed as mentioned above. The plate then subsequently incubated at 37 °C in 5 % CO^2 and read the plate at the absorbance at 450 nm using a microplate reader (Epoch, BioTek Instruments, Inc.)

2.9.3. Bone resorption assay

The bovine bone slices (thickness: 100−200 μm) were put into 96-well plates and cells were inoculated as a density of 2×10^4 cells/well. Then cells treated within extracts in 10 % RANKL (100 ng/mL) solution for 7 days to evaluate pit formation area. After that, the bone slices were washed with PBS and 2.5 % glutaraldehyde, then fixed in 4 % paraformaldehyde for 20 min. Bone resorption pits were then visualized by a scanning electron microscope (FEI Quanta 250) and the area were quantified using Image J software.

2.9.4. TRAP staining assay

RAW264.7 cells with the density of 5×10^4 cells/well were seeded on tablet samples (3 mm in height × 10 mm in diameter) of each group in a 48-well culture plate. When cell density reached 70–80 % approximately, the cells were stimulated with RANKL (Sigma, USA) supplemented in the extracts of each material group according to the commodity protocol for 7 days. After that, TRAP staining assay was performed to assess detect number of osteoclasts (TRAP-positive multinucleated cells) with optical microscope (Olympus, IX71, Japan).

2.9.5. Osteoclastogenesis-related proteins

After culturing with extracts in 10 % RANKL solution for 7 days, RAW264.7 cells were lysed and the lysates were centrifuged and the total protein concentration was detected as mentioned above. Western blotting assay was performed to evaluate the osteoclastogenic proteins expression. Primary antibodies targeting NFATc1 (1:1000), CTSK (1:1000) and GAPDH (1:1000) were used and the protein signals were visualized using the enhanced chemiluminescence system reagent as mentioned above. The relative grey value was analyzed with Image J.

2.9.6. Osteocalstogenesis-related genes

Cells were harvested and used to reverse-transcribe the RNA into cDNA as mentioned above. RT-PCR was performed to evaluate the osteoclastogenesis-related genes expression (TRAP, Rank, NFATc1, c-Src and β-actin as reference). Primer sequences information is listed in Table S3.

2.10. In vitro angiogenesis assay

2.10.1. Cell proliferation and adhesion

In this study, human umbilical vein endothelial cells (HUVECs) obtained from the Cell Bank of Shanghai Institutes for Biological Sciences were used to evaluate the angiogenesis. Cell viability was also tested adopting CCK-8 assay, Live/Dead staining assay and SEM observation as mentioned above.

2.10.2. Wound healing assay

The migration of HUVECs was identified with the wound healing assay. HUVECs were seeded in a 6-well plate with a density of 5×10^4 cells/cm^2. The monolayer was scraped with a sterile pipette tip to create a cell-free wound zone. The cells were then treated with different cement extracts and followed by microscopic evaluation of the wound width of the monolayer after 12/24 h.

2.10.3. Tube formation assay

For the tube formation assay, a 24-well plate was firstly pre-treated using polymerized Matrigel (BD Biosciences, San Jose, CA), then cells were seeded in the plate with a density 1×10^5 cells/well on the Matrigel surface and then incubated with the extract for 12 h. Microscopic images were taken at random by Image J with the Angiogenesis Analyzer plug-in (NIH, Bethesda, MD) to quantify the tubular network (number of master junctions and total segment length).

2.10.4. Angiogenesis-related gene levels

HUVECs were harvested and used to reverse-transcribe the RNA into cDNA as mentioned above. RT-PCR was performed to examine the gene expression levels of Willebrand Factor (vWF), Vascular Endothelial Growth Factor (VEGF), CD31, and β-actin was used as control reference after 3 days of culture. The sequences information is displayed in Table S4.

2.11. In vivo evaluation of the reinforced bone cements

2.11.1. OP rat models and DXA analysis

All animal experiment protocol was approved by the Animal Committee of Zhongshan Hospital, Fudan University. (Ethic approval number: Y2022-217). Thirty-six female rats (2 months old, 300 ± 30 g, Shanghai JASJ Laboratory Animals Co., Ltd., China) were housed and allowed to freely eat, drink and move. Rats received general anesthesia using pentobarbital sodium (0.1 mL/100 g, Sigma, USA).

For OP rat model induction, the rats were randomly divided into two groups: sham control group (Control, n = 4) and OVX group (OVX, n = 32). Anesthesia was induced using 4 % pentobarbital with intraperitoneal injection. After shaving the left and right dorsal hair, the skin was sterilized, and a 20 mm midline dorsal skin incision was made (Fig. S5). The wound was closed by suturing after excision of a pir of ovaries [30]. The control group rats received the same surgical procedure without the removal of ovaries. After 12 weeks, BMD was determined for a whole body on lumbar spines, femurs, and femoral condyle of rats by using dual-energy X-ray absorptiometry (DXA), and ROI analysis was conducted (Fig. S6).

2.11.2. Construction of femur defect models

The surgical area was shaved and disinfected with 75 % ethanol. A 3 cm incision was made to reveal the femoral epiphysis and a surgical drill was then applied to create bone defects (3 mm in depth) in the femoral condyles. Solidified sterilized cement specimens (CPC, C/PL/C, C/A-PL/C, C/AM-PL/C) were administrated into the defect area with a 1 mL syringe, and the layers of subcutaneous tissue were closed with absorbable sutures (Fig. S7). All rats were given an intramuscular injection of antibiotics (penicillium, Sigma, USA) after surgery at a dose of 40 mg kg for 3 days to minimize the risk of infection. The mineralization rate was investigated according to the previous work [13]. Calcein and Alizarin red were injected peritoneally at 4 and 6 weeks postoperatively. Three rats of each group were sacrificed, and the mineral apposition rate was analyzed based on the distance between the green and red fluorescence labels at 8 weeks in each group.

2.11.3. Biocompatibility evaluation of the cement

12 weeks after surgery, the harvested organs including heart, liver, spleen, lung, and liver were fixed in 10 % formalin for 24 h. Then all samples were dehydrated by graded ethanol. Sections of 300 μm thickness were allotted for tissue staining after embedding of paraffin (Beyotime Biotechnology, China) till solidification. A hematoxylin-eosin (H&E) staining assay was performed for histological observation.

2.11.4. Micro-computed tomography (Micro-CT) analysis

The femoral condyles of the rats were harvested after 6/12 weeks surgery, then fixed for 24 h in 10 % formalin. After that, samples were evaluated by Micro CT analysis (Bruker SkyScan1172, Belgium, voltage 100 KV, current 100 μA, pitch 2, filter 0.11 mm Cu). The relevant program (Micro View) was utilized to visualize and quantify bone volume fraction (BV/TV), trabecular separation (Tb. Sp), trabecular thickness (Tb. Th) and trabecular number (Tb. N).

2.11.5. Histological analysis

The femoral condyles were harvested in 12 weeks after surgery were fixed and rehydrated in grades of ethanol. After that, all samples were embedded in paraffin. Samples were embedded with methyl (Beyotime Biotechnology, China) till solidification, then 300 μm thick sections were allotted for hard tissue staining. H&E staining, Toluidine Blue (T&B) staining and Verhoeff-Van Gieson staining (V&G Staining) were performed for histological analysis.

2.11.6. Western blot

Total protein was extracted from harvest sample using RIPA (Beyotime, China). The protein of each group was then resolved by SDS-PAGE and then transferred to polyvinylidene fluoride (PVDF) membranes. PVDF membranes were incubated with osteogenesis-related indicators (OPN, 1: 500; Runx2, 1: 500) and osteoclastogenesis-related indicators (NFATc1 1:500; CTSK, 1: 500) overnight at 4 °C. After that, the membranes were incubated with secondary antibodies for 1 h at room temperature. Finally, the proteins were visualized using a chemiluminescent peroxidase substrate as mentioned as 2.8.5.

2.12. Statistical analysis

A minimum of three independent replicates were used for each experiment. The mean ± standard deviation (S.D.) was used to present continuous variables. One-way or two-way analysis of variance (ANOVA) followed by *t*-test was used to compare the different treatment groups in SPSS 20.0. The level of significant difference is set as $p^* < 0.05$ and $p^{**} < 0.01$.

3. Results and discussion

3.1. Characterization of membranes with ALN and nMgO

PLGA has good degradability, and the drugs (ALN& nMgO) loaded will be released during the degradation process to achieve a sustained release of drugs into the local environment. The overall diameter of the fibers in the electrospun membranes was less than 1 μm, while in some parts the drugs and nMgO showed agglomeration and resulted in thicker fibers (>1 μm). EDS mapping revealed a homogenous distribution of ALN and nMgO in the membranes, but the fibers occasionally showed lumps due to aggregation of ALN and nMgO particles (Fig. 1A). The FTIR spectroscopy results of electrospun films and ALN were shown in Fig. 1B. The typical absorption bands at 1758 cm^{-1} can be assigned to Carbonyl of PLGA. The peaks at 1550 cm^{-1} may be attributed to the absorption

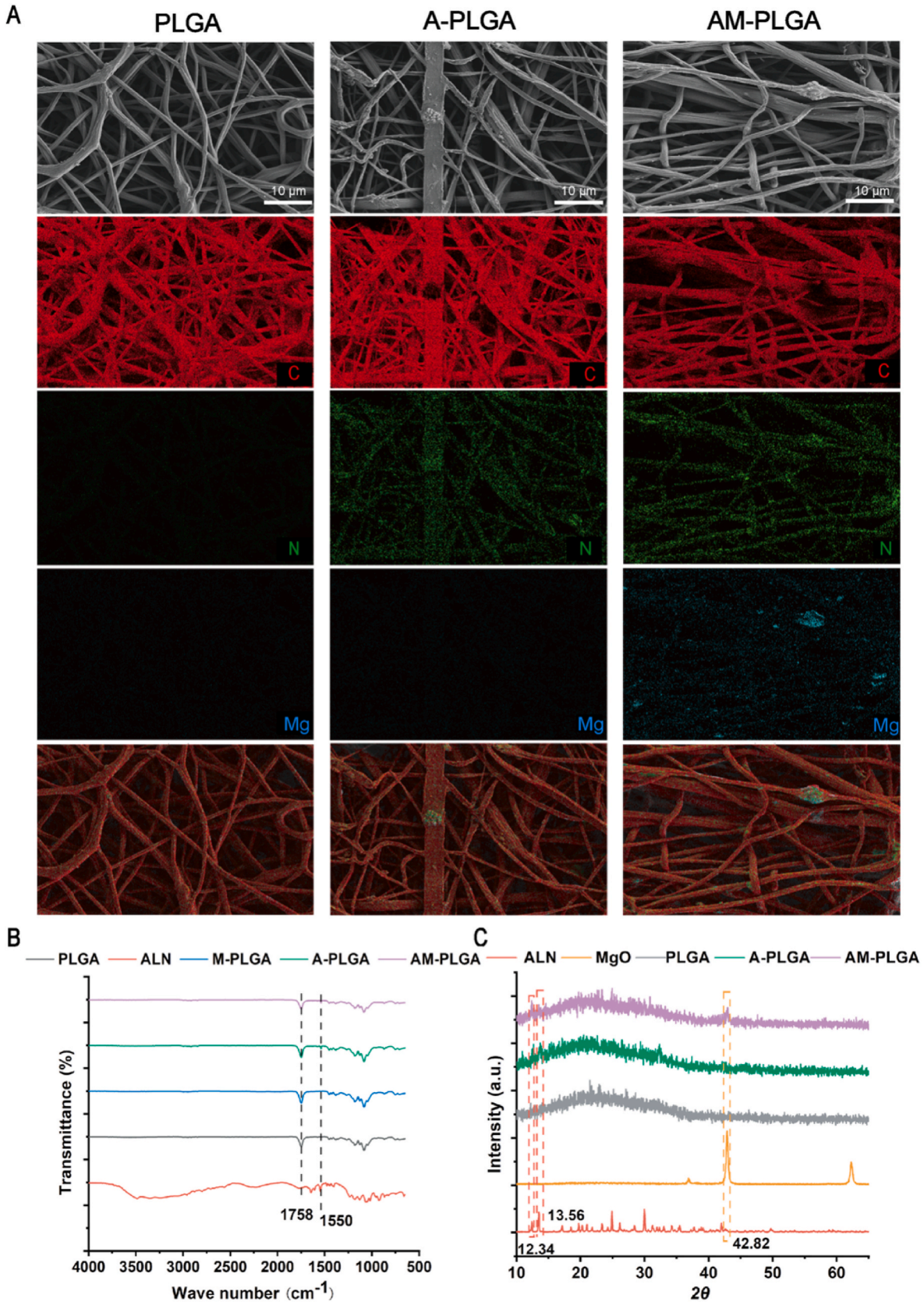

Fig. 1. Microscopic morphology and structure of membranes. (A) Surface morphology of membranes by SEM. EDS mapping of C, N, Mg element distribution on membranes surface is presented. (B) FTIR of raw materials and membranes. (C) XRD of raw materials and membranes. n = 3.

band of N–H. The XRD patterns of membranes and raw materials were presented in Fig. 1C. The sharp diffraction peak at $2\theta = 42.82°$ indicates a highly crystalline structure of MgO. PLGA was an amorphous polymer demonstrated by a broad diffraction peak at 2θ value of 22.0°. The diffractogram of the bonded film doped with ALN and nMgO also showed a broad diffraction peak. Furthermore, small crystalline peaks at $2\theta = 12.34°$ and 13.56° indicated that ALN was successfully loaded on membrane, while a sharp crystalline peak was observed at $2\theta = 42.82°$ for AM-PLGA, which demonstrated the incorporation of nMgO. Although in some membrane parts agglomeration of nMgO particles could be observed, overall, the nanoparticle was uniformly distributed in the fibers and the membrane hydrophilicity was increased (Fig. S2).

3.2. Physical and chemical properties of the composite cements

The composite cement had excellent injectability as shown in Fig. 2A, which was further improved enhance by addition of CMC (Fig. 2E). The cohesion of CPC was enhanced with the addition CMC,

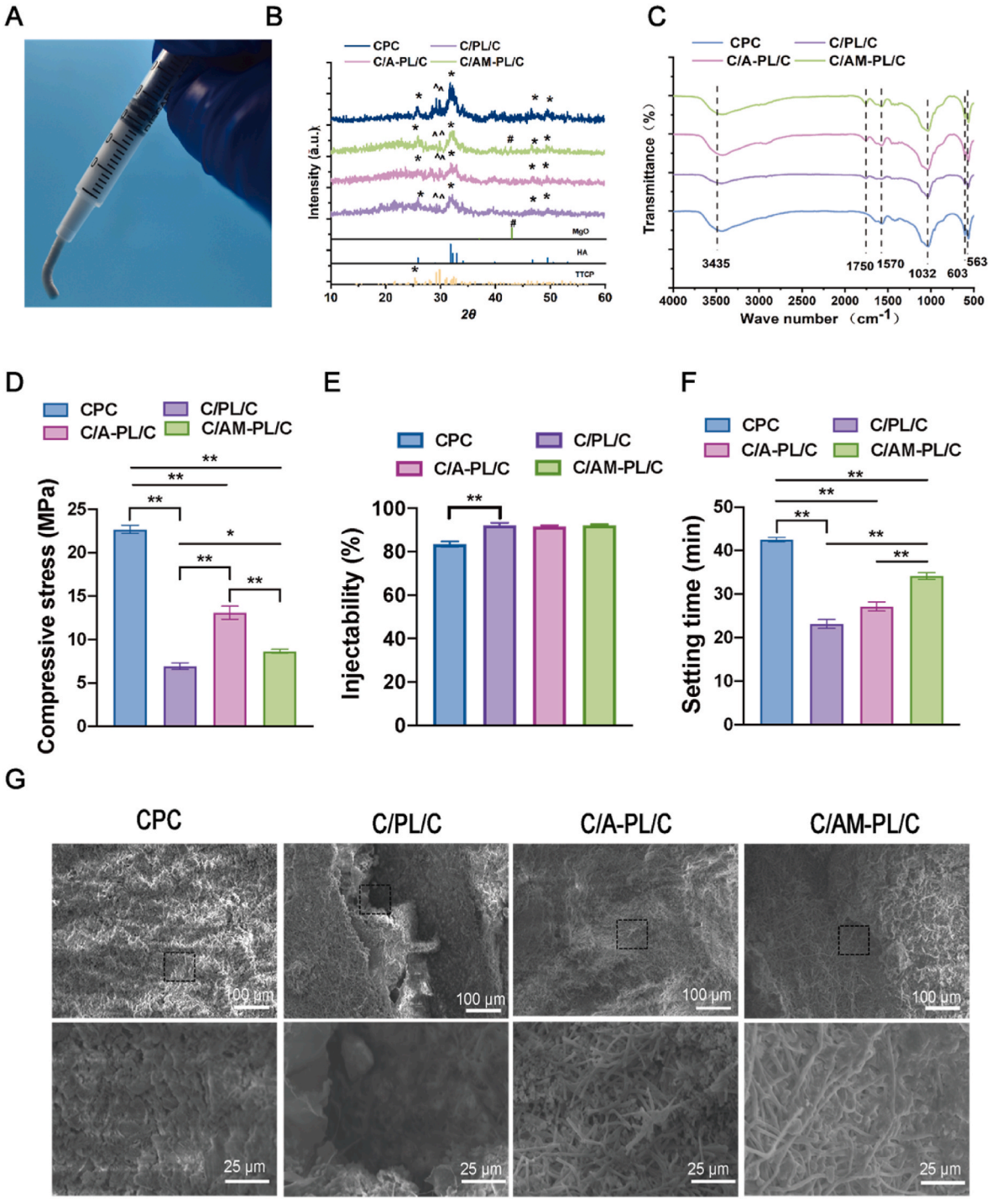

Fig. 2. Effects of a variety of fiber sheets on the operational property, structure and morphology of CPC. (A) Injectable cement diagram. (B) XRD patterns of cement samples (^: TTCP; *: HA; #: MgO); (HA: PDF#09-0432; MgO: PDF#45-0946, TTCP: PDF#25-1137.) (C) FTIR patterns of cement samples. (D) Compressive strength. (E) Injectability (%) of different cement formulations. (F) Setting time of cements. Data are presented as the mean ± SD; n = 5; *significant difference compared with control group, $*p < 0.05$ and $**p < 0.01$.

and the anti-collapse property of CPC was also effectively improved. The infrared absorption spectrum showed that, except for the 1750 cm^{-1} carbonyl group, the other peaks were essentially the same in all groups, indicating that PLGA was only blended into CPC without chemical reaction. The characteristic peak of ALN was observed, due to the low crystallinity of ALN [31]. The phase structure of each sample after curing is shown in Fig. 2B. All groups showed typical HA and unhydrated TTCP, and a smaller diffraction peak at $2\theta = 42.82^{\circ}$ in the C/AM-PL/C group, where part of the fiber-encapsulated nMgOs were released into the CPC matrix [32,33].

The mechanical properties of cement were further investigated. When added with PLGA fiber sheet and CMC, the compressive strength (Fig. 2D) of CPC decreased significantly to 6.9 ± 0.4 MPa. However, the compressive strength was 13.5 ± 0.5 MPa for C/A-PL/C and 8.6 ± 0.2 MPa for C/AM- PL/C, an increase of 95.6 % and 24.6 %, respectively, compared to the C/PL/C group. It is possible that the introduction of ALN and MgO enhances the hydrophilicity of the PLGA fiber sheets (Fig. S2), which improves the interfacial compatibility between CPC and

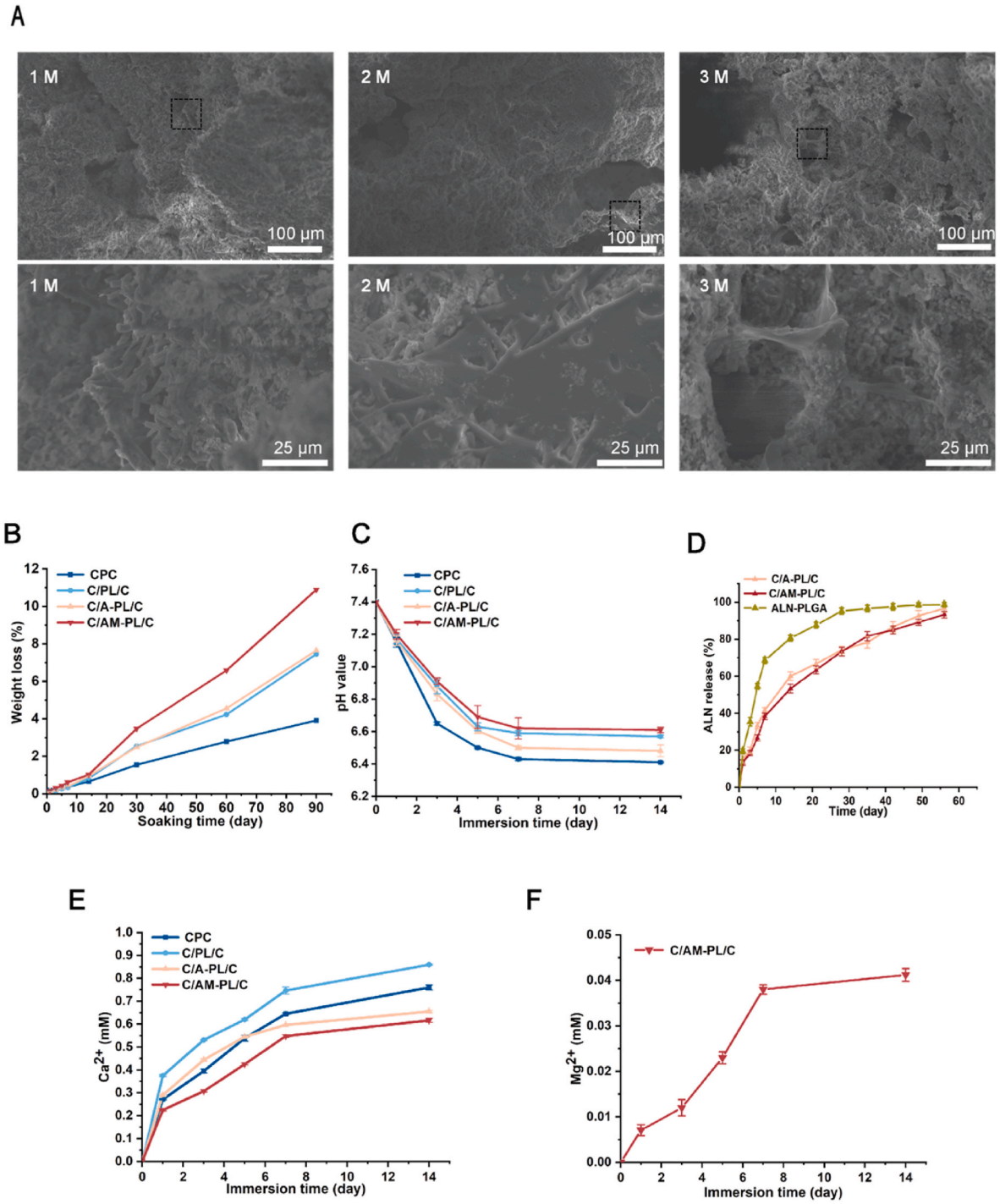

Fig. 3. Effects of different fiber sheets on the physicochemical properties of CPC. (A) Surface morphology of C/AM-PL/C samples degradation after 1 month, 2 months, and 3 months respectively. (B) Weight loss curves of samples after immersing in Tris-HCl for different time. (C) The pH vibration of PBS after cement samples soaking. (D) ALN release. (E) Ca^{2+} released into PBS determined by ICP-AES. (F) Mg^{2+} released into PBS determined by ICP-AES. Data are presented as the mean ± SD; n = 3; *significant difference compared with control group, *$p < 0.05$ and **$p < 0.01$.

PLGA fiber, leading to an increase in the compressive strength of C/A-PL/C and C/AM-PL/C [34]. Fortunately, the compression fracture work of the fiber-modified cement is higher than pure CPC. The toughness of C/A-PL/C (236.5 ± 4.1 MPa) and C/AM-PL/C (196.4 ± 2.0 MPa) was enhanced by 30.9 % and 8.6 %, respectively, compared to CPC (180 ± 5.1 MPa) (Fig. S3). The variation in setting time of different groups was analyzed and results were shown in Fig. 2F. After the addition of various types of PLGA sheet and CMC, respectively, in CPC, the solidification time was reduced to 23.2 ± 0.8 min for C/PL/C, 27.0 ± 0.8 min for C/A-PL/C, and 34.2 ± 0.6 min for C/AM-PL/C. Meanwhile when PLGA fibers and CMC were added to the CPC matrix, there was a small increase in porosity, which might also contribute to the decrease in mechanical properties (Fig. S4).

This SEM micrograph (Fig. 2G) demonstrated the bonding of the cement substrate to the different groups of PLGA after 72 h of curing. The images clearly showed that the fiber sheets of each group were uniformly distributed in the CPC, but there was severe phase separation between the PLGA fiber sheets and the CPC, resulting in the formation of large micron-sized pores. Interestingly, the phase separation was significantly reduced in the C/A-PL/C and C/AM-PL/C groups, and the crystals resulted from the CPC hydration were tightly bound between the A-PLGA fiber.

3.3. The effects of fiber sheets on the physicochemical properties of cement

SEM analysis was performed after 1, 2, and 3 months of the simulated degradation of bone cement. The results showed that the fiber morphology was relatively intact at 1 month, but the porosity of bone cement had increased. After 3 months, large areas of fiber had been destroyed. Only a few undegraded fragments remain, deposited near the orifice, leaving large pores in the cement (Fig. 3A). The degradation rate of each group for up to 90 days was presented in Fig. 3B. The degradation of PLGA can increase the porosity of CPC and increase the contact surface between CPC, which can accelerate the degradation of CPC and facilitate bone formation. Our results showed that the degradation rate of bone cement incorporated with PLGA fibers was significantly improved, which solved the problem of slow degradation of CPC. The degradation rate of C/AM-PL/C was faster than those of C/PL/C and C/A-PL/C, and the degradation rate of C/A-PL/C is almost same to that of C/PL/C. In addition to the physicochemical and mechanical properties mentioned above, the releases of ALN and Mg^{2+} during the degradation process were also monitored and quantified. The results showed that the release of ALN could last for 8 weeks, while the release of Mg^{2+} was shorter but also effective for osteogenesis according to previous publications.

To analyze the release of ALN and Mg^{2+} during the degradation process, the concentrations of ALN, Ca^{2+}, Mg^{2+} and the pH of the cement soaking solution were monitored (Fig. 3C–F). All samples showed similar pH value change trends (Fig. 3C). The pH of C/PL/C declined slightly faster compared to the C/PL/C and C/AM-PL/C, which eventually reached to 6.5 ± 0.04. As shown in Fig. 3D, ALN was almost fully released within 4weeks in the ALN-PLGA group, but the release of ALN lasted for 8 weeks with a total release over 90 %, reaching 74.2 ± 2.0 % for C/A-PL/C and 73.3 ± 2.3 % for C/AM-PL/C, respectively, in the first 4 weeks, which may be attributed to the fact that CPC also has a sustained release effect on ALN(27). The addition of ALN and nMgO can slow down the release rate of Ca^{2+}. The Ca^{2+} concentration of C/AM-PL/C was lower than that in the other group with the highest concentration reached 0.6 ± 0.01 mM. The release of Mg^{2+} was rapid in the first 7 days (with 0.038 ± 0.01 mM released within 7 days), while the Mg^{2+} concentration only reached 0.04 ± 0.01 mM by 14 days. In summary, SEM and EDS analysis showed that ALN and nMgO were successfully loading on the fibers. The drug-loaded PLGA fibers were then mixed with CPC and CMC to obtain the solid phase of injectable drug-loaded bone cement (C/AM-PL/C). The C/AM-PL/C cement was characterized by its physical and chemical properties and drug release, which demonstrated its good mechanical strength, degradability, and anti-washout property. It has also been demonstrated that the C/AM-PL/C cement can achieve successful sustained drug release under simulated degradation conditions *in vitro*.

3.4. The effects of C/AM-PL/C on cell proliferation and adhesion

The cell biocompatibility was evaluated by CCK-8 analysis, Live/Dead staining assay and SEM observation. CCK-8 results showed that both BMSCs and HUVECs proliferated well in C/AM-PL/C group (Fig. 4A and B). Live/Dead staining results also showed almost all cells were alive (Fig. 4C and D). Moreover, SEM was used to observe cell attachment on the surface of each cement, and the morphological results showed that both BMSCs and HUVECs attached and spread well on the cement surfaces (Fig. 4E and F). These results confirmed that both BMSCs and HUVECs cultured with cement extract retained normal cell morphology and good biological activity. No significant difference on cell proliferation rate could be found between the cement extract and conventional medium groups, which demonstrated that each cement had good cytocompatibility for BMSCs and HUVECs. After culturing the cells on the surface of bone cements, from SEM results, it could be observed that in C/PL/C, C/A-PL/C and C/AM-PL/C groups there were more cells growing and spreading on the surface when compared to CPC group, which can be attributed to the enhanced porosity due to PLGA degradation. These results also further confirmed the good biocompatibility of C/AM-PL/C cement. Taken together, the C/AM-PL/C was non-cytotoxic and compatible for cell adhesion and proliferation.

3.5. Effects of C/AM-PL/C cement on osteogenic differentiation of BMSCs

ALP and ARS staining are commonly used assays to evaluate cellular osteogenic differentiation capacity [35] and therefore were used in the current study. As shown in Fig. 5A and B, in 7/14 days of osteogenesis, the C/AM-PL/C group showed the strongest ALP-positive stain. Similarly (Fig. 5C), C/AM-PL/C group showed the most obvious ARS-positive bone-like nodules as compared with other groups. Furthermore, the protein levels of osteogenesis-associated markers were examined with western blotting, and the results showed that the extracts of C/AM-PL/C group significantly promoted the expression of OPN, Runx-2 and OCN (Fig. 5D). Consistent with the western blotting results, RT-PCR results also showed the expression of ALP, BMP-4, COL-1, OPN, Osterix and Runx-2 were significantly increased in the C/AM-PL/C group (Fig. 5E). These results were in accordance with the ALP and ARS staining results, suggesting that C/AM-PL/C cement has the best osteoconductive effect *in vitro*. In conclusion, these results demonstrated that C/AM-PL/C cement can promote the osteogenic of BMSCs.

3.6. Inhibition of C/AM-PL/C cement on osteoclastogenesis

RAW264.7 is a murine monocyte-macrophage cell line, which is frequently used in RANKL-induced osteoclastogenesis *in vitro* [36]. The imbalance between the osteoclast-derived bone resorption and osteoblast-derived bone formation plays a central role in bone regeneration [37]. In the current study, we evaluated the inhibitory effects of ALN on osteoclastogenesis. As shown in Fig. 6A, although osteoclasts are non-differentiated cells, the viability was apparently decreased in C/A-PL/C and C/AM-PL/C groups by using CCK-8 analysis, indicating that osteoclasts were significantly inhibited after ALN interfere. Moreover, the effects of cements on bone resorption activity of mature osteoclasts were also evaluated. Results showed that C/A-PL/C and C/AM-PL/C cement could significantly reduce the area of resorption pits (colored purple), suggesting that ALN had a positive effect on inhibiting osteoclastogenesis (Fig. 6B and C). Furthermore, as shown in Fig. 6D, TRAP staining results demonstrated that the extracts of

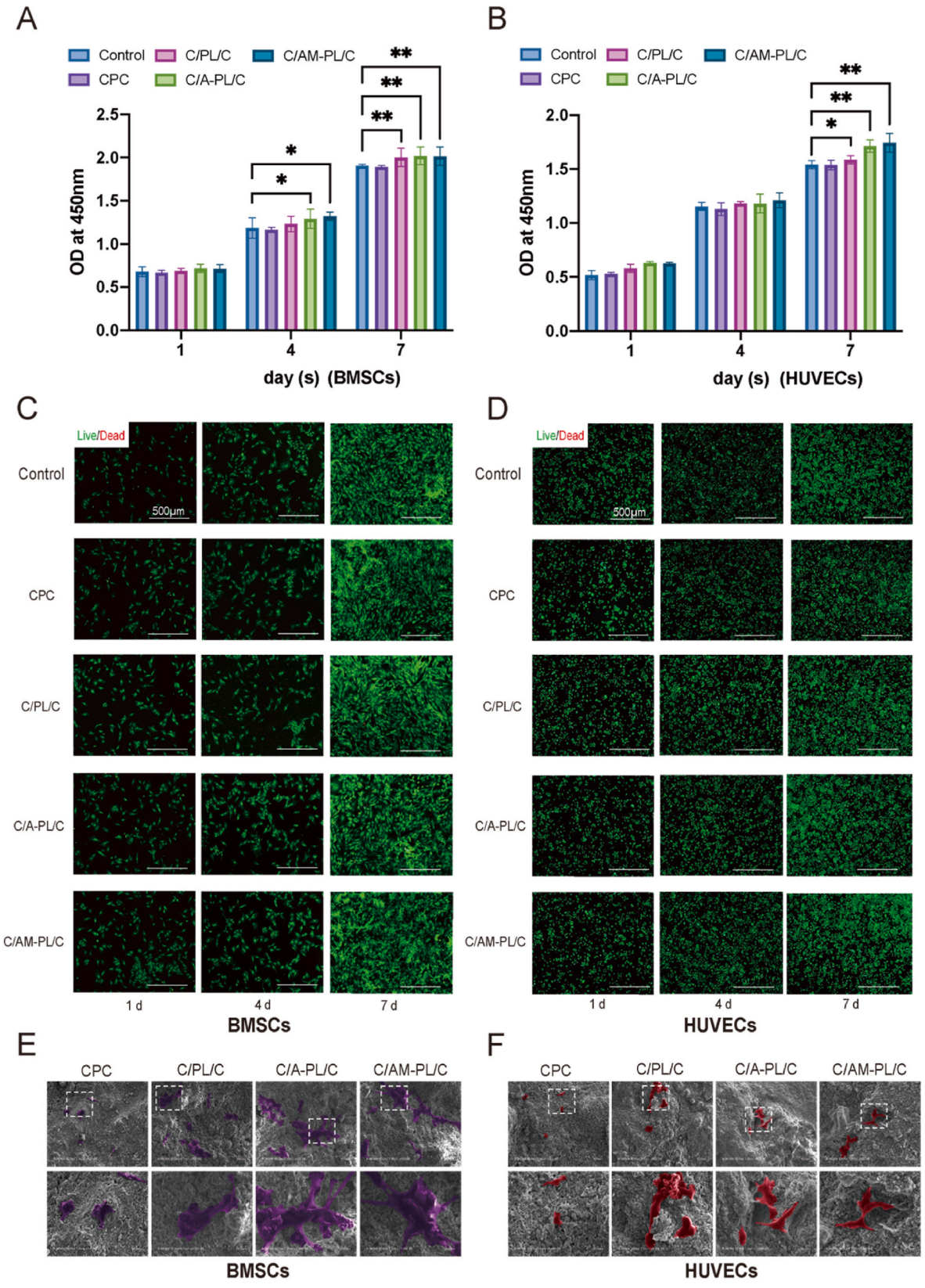

Fig. 4. Proliferation and cell adhesion of BMSCs and HUVECs treated with cement extracts. (A) CCK-8 analysis of BMSCs. (B) CCK-8 analysis of HUVECs. (C) Live/Dead staining assay of BMSCs. (D) Live/Dead staining assay of HUVECs. (E) SEM images of BMSCs on the cement surface after 24 h of incubation (BMSCs are colored purple for easy viewing). (F) SEM images of HUVECs on the cement surface after 24 h of incubation (HUVECs are colored red for easy viewing). Data are presented as the mean ± SD; n = 3; *significant difference compared with control group, *$p < 0.05$ and **$p < 0.01$. (For interpretation of the references to color in this figure legend, the reader is referred to the Web version of this article.)

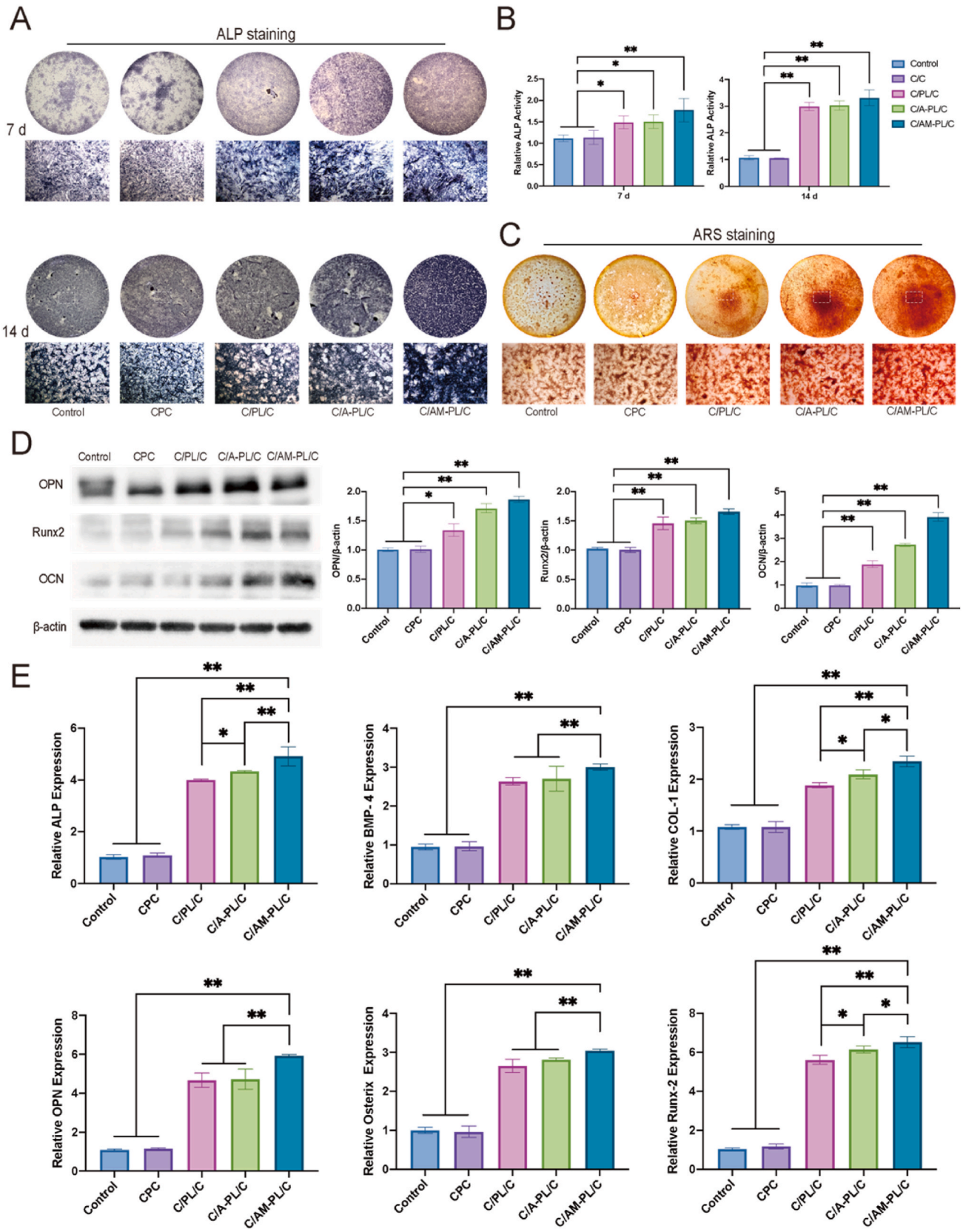

Fig. 5. Osteogenic effects on BMSCs treated with cement extracts. (A) ALP staining of BMSCs for 7 days and 14 days. (B) Quantification of ALP activity of BMSCs for 7 days and 14 days. (C) ARS staining of BMSCs for 21 days. (D) Osteogenesis related proteins expression in BMSCs cultured in cement extracts for 7 days. (E) Osteogenesis related genes expression of BMSCs cultured in cement extracts for 7 days. Data are presented as the mean ± SD; n = 3; *significant difference compared with control group, $*p < 0.05$ and $**p < 0.01$.

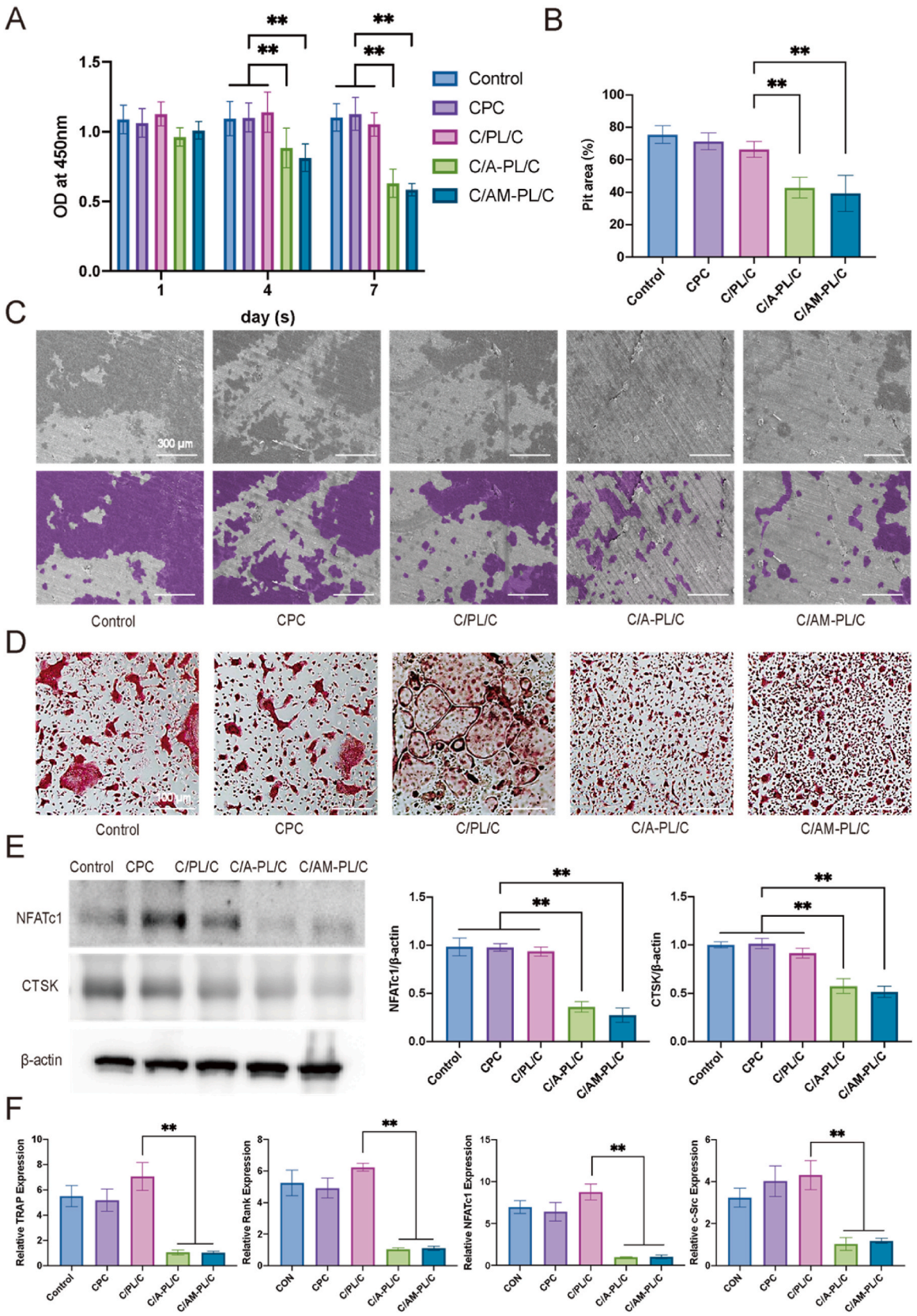

Fig. 6. Inhibitory effects of cement extracts on osteoclastogenesis. (A) Cell viability of CCK-8 results. (B–C) The bone slices of each group (resorption area is colored purple for easy viewing). (D) TRAP staining assay. (E) Protein expression levels of NFATc1 and CTSK. (F) TRAP, Rank, NFATc1 and c-Src mRNA expression levels. Data are presented as the mean ± SD; n = 3; *significant difference compared with control group, $^{*}p < 0.05$ and $^{**}p < 0.01$. (For interpretation of the references to color in this figure legend, the reader is referred to the Web version of this article.)

C/A-PL/C and C/AM-PL/C cement could inhibit osteoclastogenesis (the decrease in TRAP-positive multinucleate cells) in comparison to the control, CPC and C/PL/C groups. The western blotting results showed that the protein levels of NFATc1 and CTSK were significantly decreased in C/A-PL/C and C/AM-PL/C groups, suggesting that C/A-PL/C and C/AM-PL/C cements could attenuate the RANKL-induced osteoclast differentiation by down regulating the key proteins (Fig. 6E). Accordingly, RT-PCR results showed that the extracts of C/A-PL/C and C/AM-PL/C cement could significantly reduce the expression of osteoclastogenesis-related genes (TRAP, Rank, NFATc1 and c-Src) (Fig. 6F). Notably, a slight increase in osteoclast formation could be observed in the C/PL/C group compared to the control and CPC groups, however, there was no statistical difference between the groups, which was still consistent with the TRAP staining results and western blot analysis results. Altogether, these results demonstrated that C/A-PL/C and C/AM-PL/C could significantly inhibit osteoclastogenesis, indicating that the release of ALN function well and cooperate with Mg^{2+} and Ca^{2+} to facilitate bone regeneration.

3.7. Effects of C/AM-PL/C cement on angiogenic capacity of HUVECs

Neovascularization is a critical part during bone formation. Previous studies have demonstrated that materials can indirectly promote bone regeneration by promoting angiogenesis [29,38]. In the present study, a wound healing assay was used to evaluate the effects of cement extracts on HUVECs migration. The results showed that the HUVECs migration was significantly enhanced in the C/AM-PL/C cement group (Fig. 7A,C). Moreover, tube formation assay results showed that the C/AM-PL/C cement significantly promoted angiogenesis when compared to other groups (Fig. 7B). The number of meshes and master junction assays were adopted to quantify the tube formation capacity, where more mater junctions and increased length of total segments were detected in the C/AM-PL/C cement group (Fig. 7D). These results suggested that C/AM-PL/C could enhance the migration capability and vascularization of HUVECs. The loading of ALN and nMgO increased the node of tube formation and the total tube length. Moreover, the expression of angiogenesis-related genes was assessed by RT-PCR after 3 days' treatment. Results also showed that the C/AM-PL/C group significantly enhanced the expression of these genes as compared with other groups (Fig. 7E). Interestingly, it can also be observed that the addition of PLGA slightly promoted angiogenesis, which may be due to more Ca^{2+} and LA (the metabolite of PLGA) in the extract [39]. Altogether, these results suggested the positive effects of C/AM-PL/C cement on angiogenic capacity of HUVECs.

3.8. Rats osteoporosis model and the biocompatibility of C/AM-PL/C cement in vivo

The OP rat model was established by ovariectomy and measured by DXA at 3 months after surgery. Results showed that the rat BMD was significantly decreased, demonstrating the successful of the OP model. The femoral condyle defect model was then established in OP rat model. The CPC, C/PL/C, C/A-PL/C and C/AM-PL/C cements were injected into the bone defects to assess material osteo-integration properties and the effects on OP bone regeneration. Compared to the control group, the BMDs of OVX rats were significantly decreased not only in lumbar spines but also in femur and femoral condyles, demonstrating that OP rat model was established successfully (Fig. S8). Moreover, the biocompatibility of each cement was evaluated by using blood biochemical tests (Fig. S9) and H&E staining of the major organs (heart, liver, spleen, lung, kidney) in rats after material implantation for 12 weeks (Fig. S10). No significant difference could be found in cement groups when compared to the control, which demonstrated the good biocompatibility of bone cements *in vivo*.

3.9. Effects of C/AM-PL/C cement on OP bone regeneration

During the process of cement injection into the defect area, it was observed that the anti-washout property maintained the shape of the cement from being flushed away by blood. ALN is one of the most commonly used anti-osteoporosis drugs, which can effectively inhibit bone resorption of osteoclasts and reduce osteolysis, has been widely used in clinical practice in recent years [40–42]. Studies have reported that implemented local ALN delivery to promote bone repair by loading ALN on injectable hydrogels could effectively promote bone regeneration in osteoporotic rats *in vivo* [42,43]. It is also confirmed that loading ALN in a dual-delivery system with substance P could effectively regulate osteogenesis-osteoclastogenesis balance for promoting immediate implant osseointegration [44]. Similar to above results, in the present study, C/AM-PL/C could not only provide space for bone formation and vascular implantation but also facilitate bone regeneration via the inhibitory effects of ALN on osteoclastogenesis and the improvement of Mg^{2+} and Ca^{2+} on osteogenesis and angiogenesis based on the microporous structure of C/PL/C cement, therefore further facilitating the correction of the imbalanced bone resorption and formation in OP rat. Micro-CT was used to analyze new bone formation in the femoral condyle defects in 6 and 12 weeks after implantation (Fig. 8A). The newly-formed bone (marked as yellow) surrounding the surface of the cylindrical bone cements could be observed, and the results showed more new bone around the implants in C/A-PL/C and C/AM-PL/C groups at 6 weeks, whereas no obvious new bone formation could be found in the control, CPC and C/PL/C groups. At 12 weeks, the new bone formation was more obvious in the C/A-PL/C and C/AM-PL/C groups (Fig. 8B). The BMDs were significantly enhanced in the C/A-PL/C and C/AM-PL/C groups while the C/AM-PL/C group showed the best new bone formation effect at both 6 and 12 weeks (Fig. 8C). Similar trends were observed in BV/TV, Tb. Th and Tb. N, suggesting the best new bone microarchitecture in the C/AM-PL/C group (Fig. 8D).

To further analyze the effects of the cements on osteogenesis, H&E staining, V&G staining and T&B staining were performed. After implantation, more new bone formation could be observed in C/A-PL/C and C/AM-PL/C groups (when compared to the control, CPC and C/PL/C groups) according to the T&B staining results. The C/AM-PL/C group showed the mostly significant osteoconductive capacity among all groups. Additionally, V&G staining was also adopted to detect the response of osteocollagenous fibers surrounding the cements (Fig. 9A–C). Results showed that the C/A-PL/C and C/AM-PL/C cements were well integrated with the osteocollagenous fibers, while minimal fibrous capsules were detected in the control and CPC groups. Collectively, the C/AM-PL/C groups showed the mostly significant effects on OP bone regeneration under OP. Further, as observed using fluorescence microscopy, we investigated the bone regeneration and mineralization rates *in vivo* were evaluated using the Calcein and Alizarin labelling in femur defects of the live animals. As shown in Fig. 9B–D, the C/A-PL/C and C/AM-PL/C groups exhibited more apparent distances between green and red labels in comparison to other groups. The mineral apposition rate in the C/A-PL/C and C/AM-PL/C groups were significantly higher than that in the control, CPC and C/PL/C groups, and the C/AM-PL/C showed the best enhancement on bone mineralization rates. These results indicated that the C/AM-PL/C cement could significantly improve the bone regeneration and bone mineralization rate in OP rat. Additionally, the protein levels of osteogenesis-related markers and osteoclastogenesis-related markers were also examined with western blotting. The results showed that the extracts of C/AM-PL/C group significantly promoted the expression of OPN and Runx2 *in vivo* (Fig. S11). More importantly, the expression of osteoclastogenesis-related markers was significantly decreased after treating with C/AM-PL/C bone cement (Fig. S12). Summarily, C/AM-PL/C cement could not only inhibit osteoclast differentiation, but also facilitate bone regeneration *in vivo*, further regulating the balance of osteogenesis and osteoclastogenesis, and therefore promoting bone regeneration under

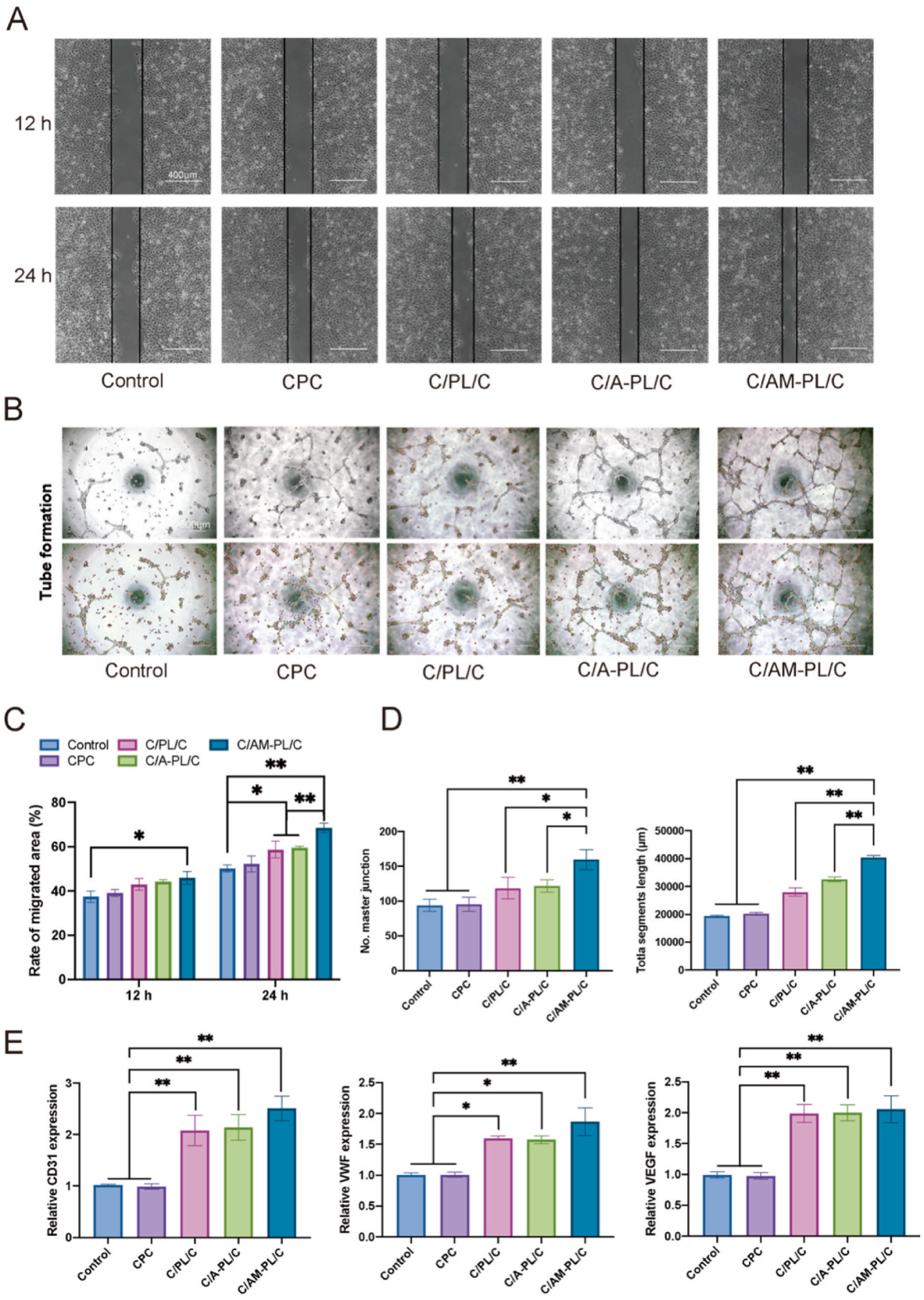

Fig. 7. Angiogenesis capacity of HUVECs treated with cement extracts. (A)Wound healing assay. (B) Tube formation assay of HUVECs cells. (C) Quantitative analysis of the wound healing assays. (D) Number of master junction and total segment length calculated with image J. (E) Angiogenesis related genes expression in HUVECs cultured in cement extracts for 3 days. Data are presented as the mean ± SD; n = 3; *significant difference compared with control group, *$p < 0.05$ and **$p < 0.01$.

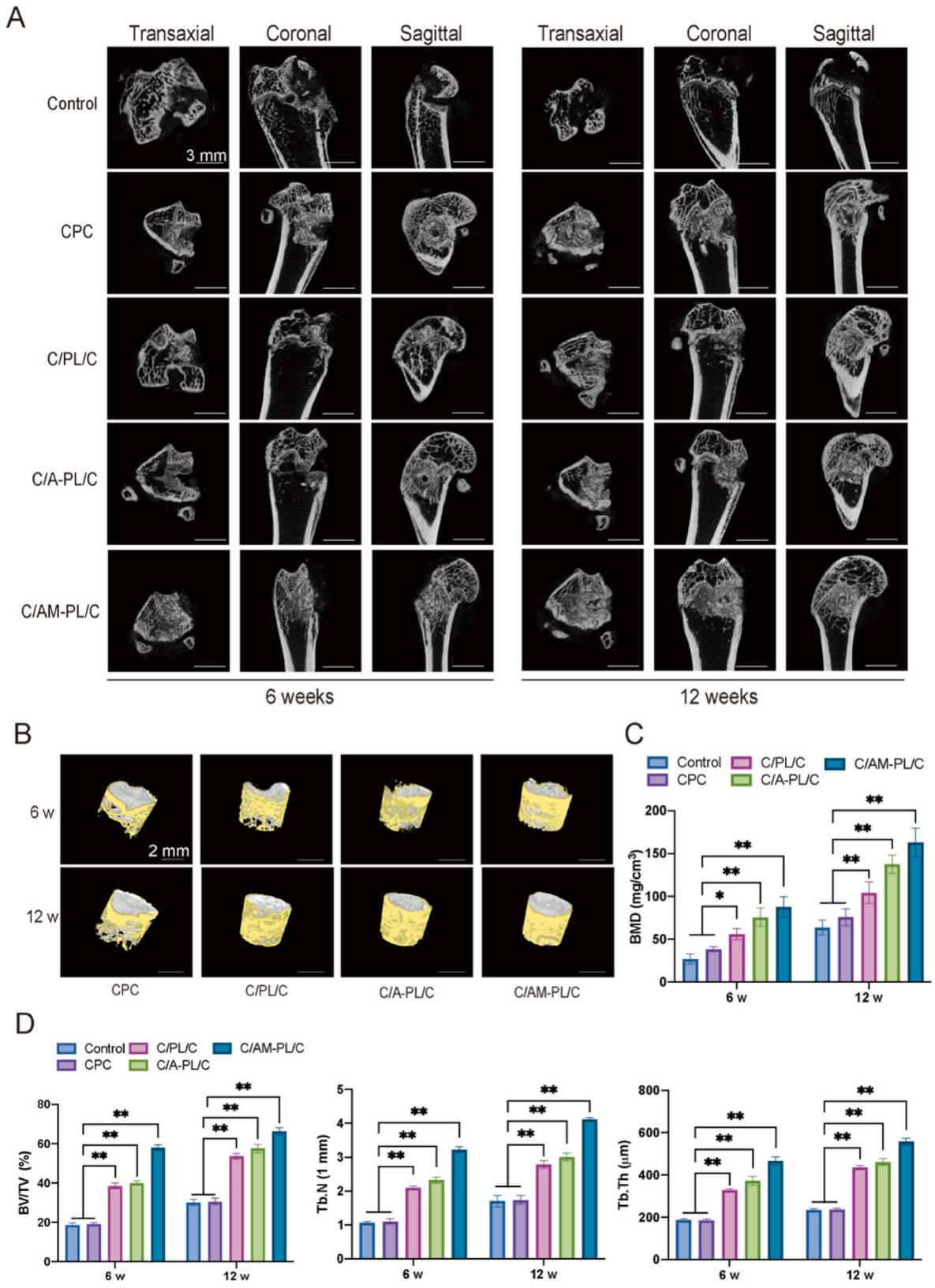

Fig. 8. The bone-healing effects of different cements in rat femoral condyle defect model *in vivo*. (A) 2D micro-CT images of rat condyle. (B) 3D reconstructions of the implants, yellow: newly formed bone; grey: cements. (C) Quantitative results of BMD. (D) BV/TV, Tb. Th and Tb. N results calculated based on micro-CT. Data are presented as the mean ± SD; n = 3; *significant difference compared with control group, $*p < 0.05$ and $**p < 0.01$. (For interpretation of the references to color in this figure legend, the reader is referred to the Web version of this article.)

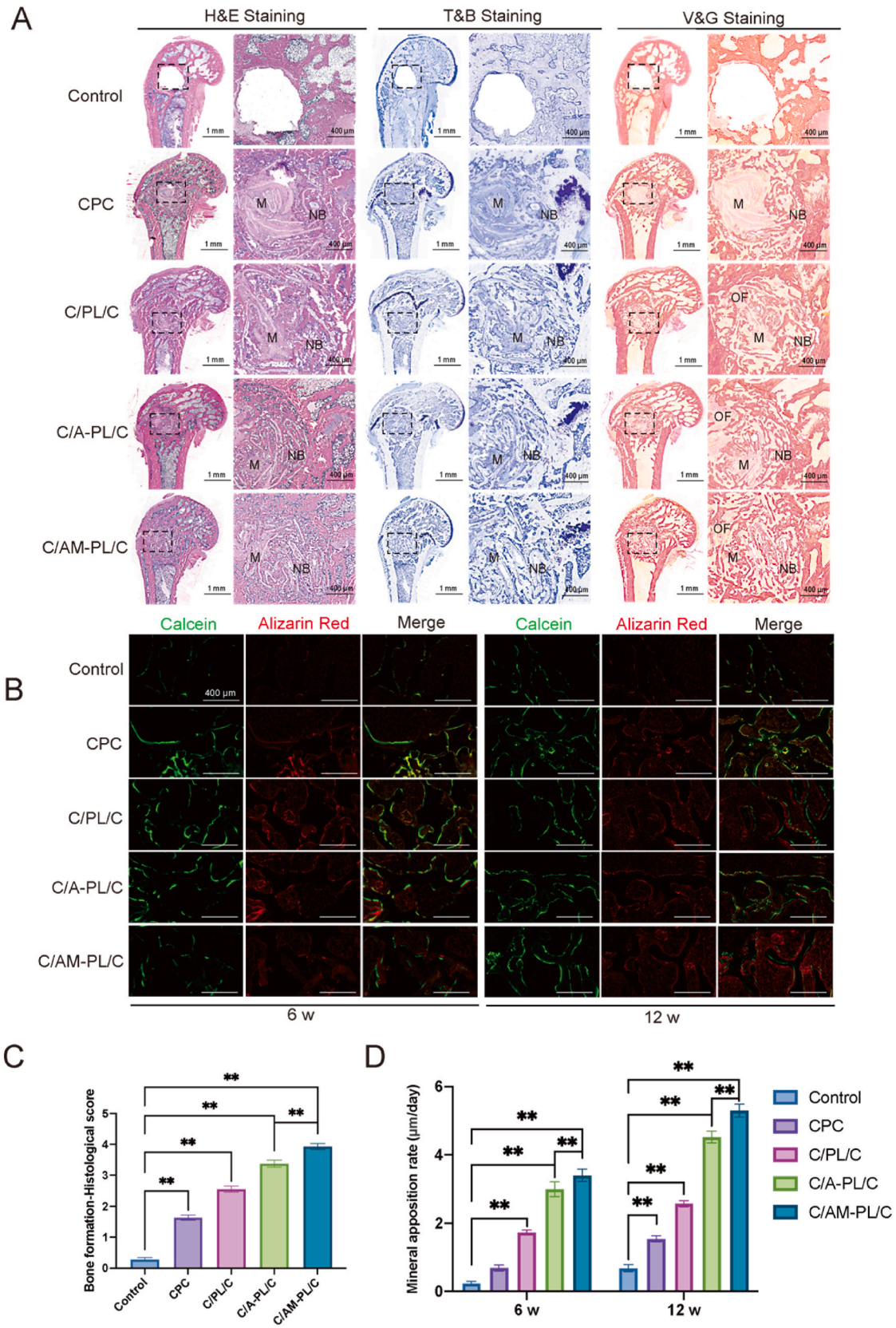

Fig. 9. Histological and fluorescent microscope observation of new bone formation after implantation. (A) Representative images of H&E, T&B and V&G staining of undecalcified femoral condyle sections, at 12 weeks after implantation. "M" refers to the cement and "NB" refers to the newly formed bone; "OF" refers to the newly formed osteocollagenous fibers. (B) Representative images of Calcein-AM and Alizarin Res staining, as observed using fluorescence microscopy at 6 and 12 weeks, respectively. (C) Histological score for new bone formation. (D) Mineral apposition rate. Data are presented as the mean ± SD; n = 3; *significant difference compared with control group, $*p < 0.05$ and $**p < 0.01$.

OP. These results demonstrated that the local drug and ion release could indeed regulate the bone regeneration in OP-related bone defects.

4. Conclusion

In summary, an injectable C/AM-PL/C bone cement that can promote osteogenesis by releasing Ca^{2+}/Mg^{2+} and inhibit osteoclastogenesis by ALN was successfully developed. The C/AM-PL/C cement exhibited good biocompatibility, anti-washout ability, degradability and effective sustained drug release capacity. The release of Ca^{2+} and Mg^{2+} owing to material degradation and the addition of nMgO can promote the osteogenesis of BMSCs and angiogenesis of HUVECs. Moreover, the release of ALN could inhibit osteoclastogenesis, further suppressing bone resorption and facilitate bone regeneration under OP by correcting the imbalanced bone resorption and formation. The effect of C/AM-PL/C cement on osteoporotic bone defects healing was further verified *in vivo*, suggesting that the novel strategy developed in this study shall benefit osteoporotic bone regeneration by enhancing the mechanical robustness and anti-washout capacity of injectable calcium phosphate cement, which showing promising high potential for minimally-invasive bone regeneration in clinical treatment.

CRediT authorship contribution statement

Lei Huang: Writing – original draft, Formal analysis, Data curation, Conceptualization. **Peihao Cai:** Formal analysis, Data curation. **Mengxuan Bian:** Methodology, Data curation, Conceptualization. **Jieqin Yu:** Methodology, Investigation. **Lan Xiao:** Resources. **Shunyi Lu:** Supervision. **Jiayi Wang:** Investigation. **Weisin Chen:** Validation. **Xingdong Xiang:** Validation. **Libo Jiang:** Visualization, Validation, Supervision. **Yulin Li:** Visualization, Validation, Supervision, Resources. **Jian Zhang:** Writing – review & editing, Visualization, Supervision, Funding acquisition.

Declaration of competing interest

The authors declared that they have no known competing financial interests or personal relationships that could have appeared to influence the work reported in this work.

Data availability

Data will be made available on request.

Acknowledgments

This work was supported by the National Natural Science Foundation of China, (No.81870965), National Key Research and Development Program (2022YFC2405802), "Technology Innovation Action Plan" of Shanghai Science and Technology Commission (21S11902700), Natural Science Foundation of Shanghai (21ZR1412300), National Key R&D Program of China (2020YFC2008400).

Appendix A. Supplementary data

Supplementary data to this article can be found online at https://doi.org/10.1016/j.mtbio.2024.101092.

References

[1] Xiao L, Zhong M, Huang Y, Zhu J, Tang W, Li D, et al. Puerarin alleviates osteoporosis in the ovariectomy-induced mice by suppressing osteoclastogenesis via inhibition of TRAF6/ROS-dependent MAPK/NF-κB signaling pathways. Aging.12(21):21706-29.

[2] Q. Chen, J. Li, F. Han, Q. Meng, H. Wang, Q. Wei, et al., A multifunctional composite hydrogel that rescues the ROS microenvironment and guides the immune response for repair of osteoporotic bone defects, Adv. Funct. Mater. 32 (27) (2022) 2201067.

[3] B. Häussler, H. Gothe, D. Göl, G. Glaeske, L. Pientka, D. Felsenberg, Epidemiology, treatment and costs of osteoporosis in Germany—the BoneEVA Study, Osteoporos. Int. 18 (1) (2007) 77–84.

[4] A. Lode, C. Heiss, G. Knapp, J. Thomas, B. Nies, M. Gelinsky, et al., Strontium-modified premixed calcium phosphate cements for the therapy of osteoporotic bone defects, Acta Biomater. 65 (2018) 475–485.

[5] N. Lee, M. Kang, T. Kim, D. Yoon, N. Mandakhbayar, S. Jo, et al., Dual actions of osteoclastic-inhibition and osteogenic-stimulation through strontium-releasing bioactive nanoscale cement imply biomaterial-enabled osteoporosis therapy, Biomaterials 276 (2021) 121025.

[6] E. Yong, S. Logan, Menopausal osteoporosis: screening, prevention and treatment, Singap. Med. J. 62 (4) (2021) 159–166.

[7] J. Zhu, S. Yang, K. Cai, S. Wang, Z. Qiu, J. Huang, et al., Bioactive poly (methyl methacrylate) bone cement for the treatment of osteoporotic vertebral compression fractures, Theranostics 10 (14) (2020) 6544–6560.

[8] I.A. Grafe, M. Baier, G. Nöldge, C. Weiss, K. Da Fonseca, J. Hillmeier, et al., Calcium-phosphate and polymethylmethacrylate cement in long-term outcome after kyphoplasty of painful osteoporotic vertebral fractures, Spine 33 (11) (2008).

[9] W. Zhi, X. Wang, D. Sun, T. Chen, B. Yuan, X. Li, et al., Optimal regenerative repair of large segmental bone defect in a goat model with osteoinductive calcium phosphate bioceramic implants, Bioact. Mater. 11 (2022) 240–253.

[10] H.H.K. Xu, P. Wang, L. Wang, C. Bao, Q. Chen, M.D. Weir, et al., Calcium phosphate cements for bone engineering and their biological properties, Bone Research 5 (1) (2017) 17056.

[11] F.C.J. van de Watering, P. Laverman, V.M. Cuijpers, M. Gotthardt, E. M. Bronkhorst, O.C. Boerman, et al., The biological performance of injectable calcium phosphate/PLGA cement in osteoporotic rats, Biomed. Mater. 8 (3) (2013) 035012.

[12] L. Schröter, F. Kaiser, S. Stein, U. Gbureck, A. Ignatius, Biological and mechanical performance and degradation characteristics of calcium phosphate cements in large animals and humans, Acta Biomater. 117 (2020) 1–20.

[13] P. Cai, S. Lu, J. Yu, L. Xiao, J. Wang, H. Liang, et al., Injectable nanofiber-reinforced bone cement with controlled biodegradability for minimally-invasive bone regeneration, Bioact. Mater. 21 (2023) 267–283.

[14] Q. Zhou, Z. Guan, S. Liu, Y. Xuan, G. Han, H. Chen, et al., The effects of metformin and alendronate in attenuating bone loss and improving glucose metabolism in diabetes mellitus mice, Aging 14 (1) (2022) 272–285.

[15] Q. Zhou, Z. Guan, S. Liu, Y. Xuan, G. Han, H. Chen, et al., The effects of metformin and alendronate in attenuating bone loss and improving glucose metabolism in diabetes mellitus mice, Aging (Albany NY) 14 (1) (2022) 272–285.

[16] M. Li, Z. Zhang, Q. Xue, Q. Li, X. Jin, J. Dong, et al., Efficacy of generic teriparatide and alendronate in Chinese postmenopausal women with osteoporosis: a prospective study, Arch. Osteoporosis 17 (1) (2022) 103.

[17] L.S. Dolci, S. Panzavolta, P. Torricelli, B. Albertini, L. Sicuro, M. Fini, et al., Modulation of Alendronate release from a calcium phosphate bone cement: an in vitro osteoblast-osteoclast co-culture study, Int. J. Pharm. 554 (2019) 245–255.

[18] Z. Shen, T. Yu, J. Ye, Microstructure and properties of alendronate-loaded calcium phosphate cement, Mater. Sci. Eng. C 42 (2014) 303–311.

[19] Y.-H. Li, Z.-D. Wang, W. Wang, C.-W. Ding, H.-X. Zhang, J.-M. Li, The biocompatibility of calcium phosphate cements containing alendronate-loaded PLGA microparticles in vitro, Exp. Biol. Med. 240 (11) (2015) 1465–1471.

[20] N.-Y.T. Nguyen, N. Grelling, C.L. Wetteland, R. Rosario, H. Liu, Antimicrobial activities and mechanisms of magnesium oxide nanoparticles (nMgO) against pathogenic bacteria, yeasts, and biofilms, Sci. Rep. 8 (1) (2018) 16260.

[21] X. Liu, X. He, D. Jin, S. Wu, H. Wang, M. Yin, et al., A biodegradable multifunctional nanofibrous membrane for periodontal tissue regeneration, Acta Biomater. 108 (2020) 207–222.

[22] Y. Zhao, S. Wang, Q. Guo, M. Shen, X. Shi, Hemocompatibility of electrospun halloysite nanotube- and carbon nanotube-doped composite poly(lactic-co-glycolic acid) nanofibers, J. Appl. Polym. Sci. 127 (6) (2013) 4825–4832.

[23] S. Pina, P.M. Torres, F. Goetz-Neunhoeffer, J. Neubauer, J.M.F. Ferreira, Newly developed Sr-substituted α-TCP bone cements, Acta Biomater. 6 (3) (2010) 928–935.

[24] F. Chen, Z. Song, C. Liu, Fast setting and anti-washout injectable calcium–magnesium phosphate cement for minimally invasive treatment of bone defects, J. Mater. Chem. B 3 (47) (2015) 9173–9181.

[25] Lacerda Schickert S. de, J.C. Pinto, J. Jansen, S.C.G. Leeuwenburgh, J.J.J.P. van den Beucken, Tough and injectable fiber reinforced calcium phosphate cement as an alternative to polymethylmethacrylate cement for vertebral augmentation: a biomechanical study, Biomater. Sci. 8 (15) (2020) 4239–4250.

[26] S.-H. Kwon, Y.-K. Jun, S.-H. Hong, I.-S. Lee, H.-E. Kim, Y.Y. Won, Calcium phosphate bioceramics with various porosities and dissolution rates, J. Am. Ceram. Soc. 85 (12) (2002) 3129–3131.

[27] C.I.A. van Houdt, P.R. Gabbai-Armelin, P.M. Lopez-Perez, D.J.O. Ulrich, J. A. Jansen, A.C.M. Renno, et al., Alendronate release from calcium phosphate cement for bone regeneration in osteoporotic conditions, Sci. Rep. 8 (1) (2018) 15398.

[28] E.A. Taha, N.F. Youssef, Spectrophotometric determination of some drugs for osteoporosis, Chem. Pharm. Bull. 51 (12) (2003) 1444–1447.

[29] Z. Hu, J. Lu, T. Zhang, H. Liang, H. Yuan, D. Su, et al., Piezoresistive MXene/Silk fibroin nanocomposite hydrogel for accelerating bone regeneration by Re-establishing electrical microenvironment, Bioact. Mater. 22 (2023) 1–17.

[30] J. Li, X. Li, D. Liu, K. Hamamura, Q. Wan, S. Na, et al., eIF2α signaling regulates autophagy of osteoblasts and the development of osteoclasts in OVX mice, Cell Death Dis. 10 (12) (2019) 921.
[31] C.I.A. van Houdt, P.R. Gabbai-Armelin, P.M. Lopez-Perez, D.J.O. Ulrich, J. A. Jansen, A.C.M. Renno, et al., Alendronate release from calcium phosphate cement for bone regeneration in osteoporotic conditions, Sci. Rep. 8 (1) (2018) 15398.
[32] N.W. Kucko, W. Li, M.A. García Martinez, Iu Rehman, A.-S.T. Ulset, B. E. Christensen, et al., Sterilization effects on the handling and degradation properties of calcium phosphate cements containing poly (D,L-lactic-co-glycolic acid) porogens and carboxymethyl cellulose, J. Biomed. Mater. Res. B Appl. Biomater. 107 (7) (2019) 2216–2228.
[33] J. Zhang, H. Zhou, K. Yang, Y. Yuan, C. Liu, RhBMP-2-loaded calcium silicate/calcium phosphate cement scaffold with hierarchically porous structure for enhanced bone tissue regeneration, Biomaterials 34 (37) (2013) 9381–9392.
[34] N.W. Kucko, D.G. Petre, M. de Ruiter, R.P. Herber, S.C.G. Leeuwenburgh, Micro- and macromechanical characterization of the influence of surface-modification of poly(vinyl alcohol) fibers on the reinforcement of calcium phosphate cements, J. Mech. Behav. Biomed. Mater. 109 (2020) 103776.
[35] D. Yan, J. Tang, L. Chen, B. Wang, S. Weng, Z. Xie, et al., Imperatorin promotes osteogenesis and suppresses osteoclast by activating AKT/GSK3 β/β-catenin pathways, J. Cell Mol. Med. 24 (3) (2020) 2330–2341.
[36] H. Hu, X. Wang, Y. Huang, B. He, J. Zhu, K. Sun, et al., Obacunone inhibits RANKL/M-CSF-mediated osteoclastogenesis by suppressing integrin- FAK-Src signaling, Cytokine 164 (2023) 156134.
[37] P. Liu, W. Wang, Z. Li, Y. Li, X. Yu, J. Tu, et al., Ferroptosis: a new regulatory mechanism in osteoporosis, Oxid. Med. Cell. Longev. 2022 (2022) 2634431.
[38] A. Marrella, T. Lee, D. Lee, S. Karuthedom, D. Syla, A. Chawla, et al., Engineering vascularized and innervated bone biomaterials for improved skeletal tissue regeneration, Mater. Today 21 (4) (2018) 362–376.
[39] J. Véras, C. Cardoso, S. Puga, A. de Melo Bisneto, R. Roma, R. Santos Silva, et al., Lactose-binding lectin from Vatairea macrocarpa seeds induces in vivo angiogenesis via VEGF and TNF-α expression and modulates in vitro doxorubicin-induced genotoxicity, Biochimie 194 (2022) 55–66.
[40] T. Tutaworn, J.W. Nieves, Z. Wang, J.E. Levin, J.E. Yoo, J.M. Lane, Bone loss after denosumab discontinuation is prevented by alendronate and zoledronic acid but not risedronate: a retrospective study, Osteoporos. Int. 34 (3) (2023) 573–584.
[41] D. Willems, M.K. Javaid, R. Pinedo-Villanueva, C. Libanati, A. Yehoshua, M. Charokopou, Importance of time point-specific indirect treatment comparisons of osteoporosis treatments: a systematic literature review and network meta-analyses, Clin. Therapeut. 44 (1) (2022) 81–97.
[42] W.A. Camargo, J.W. Hoekstra, J.A. Jansen, J. van den Beucken, Influence of bisphosphonate treatment on bone substitute performance in osteoporotic conditions, Clin. Implant Dent. Relat. Res. 25 (3) (2023) 490–501.
[43] S. Chang, C. Li, N. Xu, J. Wang, Z. Jing, H. Cai, et al., A sustained release of alendronate from an injectable tetra-PEG hydrogel for efficient bone repair, Front. Bioeng. Biotechnol. 10 (2022) 961227.
[44] H. Ji, Y. Wang, H. Liu, Y. Liu, X. Zhang, J. Xu, et al., Programmed core-shell electrospun nanofibers to sequentially regulate osteogenesis-osteoclastogenesis balance for promoting immediate implant osseointegration, Acta Biomater. 135 (2021) 274–288.